

Nanosized Lithium Aluminate (γ -LiAlO₂) Synthesized by EDTA-citrate Complexing Method, Using Different Thermal Conditions

Oscar Ovalle-Encinia¹, Heriberto Pfeiffer¹, José Artemio Fabián-Anguiano², José Ortiz-Landeros^{2,*}

¹Laboratorio de Físicoquímica y Reactividad de Superficies (LaFReS), Instituto de Investigaciones en Materiales, Universidad Nacional Autónoma de México, Circuito exterior s/n, Cd Universitaria, Del. Coyoacán, CP 04510, Ciudad de México, Mexico.

²Departamento de Ingeniería en Metalurgia y Materiales, Escuela Superior de Ingeniería Química e Industrias Extractivas, Instituto Politécnico Nacional, UPALM, Av. IPN s/n, CP 07738, Ciudad de México, Mexico.

*Corresponding author: José Ortiz-Landeros, e-mail: jortizla@ipn.mx Phone number: (55) 57296000, ext.54267

Received July 13th, 2018; Accepted October 10th, 2019.

DOI: <http://dx.doi.org/10.29356/jmcs.v63i4.1030>

Abstract. Lithium aluminate (LiAlO₂) polymorphs have been synthesized by solid-state reaction, but these ceramics usually show certain limitations attributed to the low control on the particle size, morphology and specific surface area. In this sense, different chemical synthesis pathways, citrate precursor among them, have been studied to obtain ultrafine powders exhibiting enhanced textural and morphological features. Synthesis by citrate precursor method would involve the use of alternative chelating agents for the formation of more stable metal-chelate species, such as ethylene-diamine-tetra-acetic acid (EDTA). Thus, the aim of this work was to study the γ -LiAlO₂ synthesis by EDTA-citrate complexing approach to establish the effect of the synthesis route on the structural and microstructural characteristics of the resultant powders. The synthesized ceramic powders were calcined (600-900°C) and characterized by simultaneous TG-DTA, XRD, SEM, TEM and N₂ adsorption-desorption techniques. Crystallization transition process from the precursors to the γ -LiAlO₂ phase is reported. Results show that chemical synthesis by EDTA-citrate complexing method can produce pure and crystalline γ -LiAlO₂ nanoparticles at relative low temperatures (700 °C). The possible formation mechanism is discussed.

Keywords: Ceramics; inorganic compounds; chemical synthesis; LiAlO₂.

Resumen. El aluminato de litio (LiAlO₂) en sus diferentes fases polimórficas se ha sintetizado por la técnica convencional de reacción en estado sólido; sin embargo, este método presenta ciertas limitaciones desde el punto de vista del control que se tiene en el tamaño de partícula, morfología y área específica. En este sentido, se han estudiado diferentes rutas de síntesis química para la obtención de polvos ultrafinos que presenten propiedades texturales y características morfológicas mejoradas. Entre éstas, se encuentra la síntesis por citratos precursores; un método que además del ácido cítrico, puede involucrar el uso de agentes complejantes o quelantes alternativos para promover la formación de especies más estables. Un ejemplo de lo anterior es el ácido etilendiaminotetraacético o EDTA por sus siglas en inglés. El objetivo de este trabajo es estudiar la síntesis del γ -LiAlO₂ por el método del citrato precursor-EDTA y establecer el efecto de la ruta de síntesis sobre las características estructurales y microestructurales de los compuestos obtenidos. Los polvos cerámicos sintetizados fueron calcinados a diferentes temperaturas (600-900 °C) y caracterizados por diferentes técnicas como ATG-ATD, DRX, MEB, MET y adsorción-desorción de N₂ a baja presión. Se estudió el proceso de descomposición y cristalización de los precursores hasta la obtención del óxido metálico de aluminato de litio. Los resultados muestran que el método de síntesis propuesto es adecuado para la obtención, a baja temperatura

(700 °C), de nanopartículas de la fase cristalina y pura del γ -LiAlO₂. Se discute un posible mecanismo de formación del compuesto de estudio a partir de los geles precursores usados.

Palabras clave: Cerámicos; compuestos inorgánicos; síntesis química; LiAlO₂.

Introduction

Lithium-containing ceramics find various technological applications such as tritium breeding materials [1-3], ionic conductors in the fabrication of solid electrolytes, separators and cathode materials for Li-ion batteries [4-7]. Other technological applications are the fabrication of phosphors [8,9], catalysts [10,11] and sorbents for the selective CO₂ capture [12,13]. Among these ceramics, different polymorphs of lithium monoaluminate (α -, β - and γ -LiAlO₂) have been the subject of several studies [14-25]. For example, LiAlO₂ has been reported as a good candidate as host matrix for neutron scintillators [14,15], as electrolyte matrix in molten carbonate fuel cells [16-19], as well as a candidate for certain luminescent devices [20,21] and heterogeneous catalyst for biodiesel production, [25] among others.

Specifically, γ -LiAlO₂ has been synthesized by the conventional solid-state reaction method [25-27]. However, the well-known limitations attributed to this technique are evident from the point of view of the low control on the particle sizes, low specific surface area values and the crystallization of secondary phases as impurities, among others. The aforesaid issues are matter of study since the improvement of these powders' characteristics can be valuable to expand the scope of novel applications of γ -LiAlO₂.

In this sense, different chemical synthesis pathways have been studied to obtain γ -LiAlO₂ ultrafine powders exhibiting the desirable textural and morphological features for specific uses. Some of these synthesis routes include hydrothermal [23], sol-gel [20,27], and combustion related techniques [28]. Citrate precursor is a modified sol-gel process, which also involves a combustion stage for the chemical synthesis of fine ceramic oxide powders [29-31]. Briefly, this method is based on the formation of metal complexes by using citric acid as chelating agent. The precursor solution, resulting from metal nitrates and citric acid, gives place to a highly viscous gel formed by solvent evaporation. After gelation and drying, the gel is heated, and the so-called self-ignition process occurs to calcine the organic constituents with the consequently oxide particles formation [29]. The homogeneity and stability of the gel precursor is crucial to avoid segregation and precipitation of undesirable metal-containing species and therefore to guarantee the purity of the final products. Numerous variants of the citrate method involve the use of alternative chelating agents for the formation of stable metal-chelate species [31]. For example, ethylene-diamine-tetra-acetic acid (EDTA) is a complexing agent with four carboxylate groups that provides to the molecules a higher capability to bind almost any cation in a wider range of pH than that presented by the citric acid [29]. Despite the EDTA-citrate precursor method is a promising pathway to produce LiAlO₂ particles at relative low temperatures, there isn't a detailed discussion about this specific synthesis approach for the preparation of LiAlO₂ oxides. Therefore, the aim of this work was to systematically study the preparation of pure and crystalline γ -LiAlO₂ powders by EDTA-citrate complexing approach, investigating the thermochemical behavior of the metallic EDTA-citrate precursors towards the formation of the γ -LiAlO₂ powder as well as to establish the effect of the synthesis route on both, the structural and microstructural characteristics of the resultant material.

Experimental

Materials and methods

Synthesis of materials

LiAlO₂ was synthesized by the combined EDTA-Citrate complexing method. Firstly, stoichiometric amounts of the corresponding metal nitrates, i.e., lithium nitrate anhydrous (LiNO₃ 99.0%, Alfa-Aesar) and aluminum nitrate nonahydrated (Al(NO₃)₃·9H₂O 98%, Sigma-Aldrich) were dissolved in deionized water. The

solution was heated to 70 °C and stirred during 1 h. Anhydrous citric acid (C₆H₈O₇ 99.98%, Sigma-Aldrich) and EDTA (C₁₀H₁₆N₂O₈ 98.5%, Sigma-Aldrich) were separately dissolved in an ammonium hydroxide dissolution (NH₄OH 28-30%, Sigma-Aldrich), controlling the pH value at around 9. Then, these two solutions were heated to 70 °C under stirring and subsequently dropped simultaneously to the aqueous metal nitrates-containing solution. The pH of the resultant solution was monitored and kept at around 9 by dropping an excess of aqueous ammonia solution. The molar ratio was 1:1:1.5 for metal cations: citric acid: EDTA. A transparent solution was obtained and subsequently heated to 90 °C, while it was stirred. After water evaporation, a viscous gel was obtained.

The synthesis conditions above mentioned were established with based on the construction and analysis of the chemical equilibrium diagrams by using the Hydra-Medusa software [35].

Then, the gel was heated to 300 °C to remove organic compounds. The gel burns itself on a hot plate because of the exothermic nature of this process. After calcination processes, the as-burnt sample was a dark grey powder, which was separated in four sets and subsequently calcined at 600, 700, 800 and 900 °C for 10 h. Calcination temperatures were established based on the TG-DT analysis.

Materials characterization

Firstly, the gel sample was analyzed by simultaneous thermogravimetric (TG) and differential thermal analyses (DTA). Then, gel and calcined samples were characterized by X-ray diffraction (XRD), scanning (SEM) and transmission (TEM) electron microscopies, as well as N₂ adsorption-desorption measurements.

Simultaneous TG-DT analyses were performed to determine the evolution of the chemical reaction during the synthesis of the LiAlO₂ powders. Those experiments were made on a simultaneous thermal analyzer instrument model STA 2500 Regulus of Netzsch. For these purposes, the gel samples were dynamically heated from 30 to 700 °C at 5 °C min⁻¹, using a flow rate of 60 mL·min⁻¹ of dried air.

FT-IR spectra were recorded by using a Bruker Alpha spectrometer equipped with an ATR module. A diffractometer (Bruker, D8 Advance) with Cu-K α (1.54059 Å) radiation source operating at 34 kV and 30 mA was used to identify the crystalline phases after the different thermal treatments. Samples were measured in a 2-theta range of 20-120 ° with a step size of 0.02°. Crystalline phases were identified using the Joint Committee Powder Diffraction Standards (JCPDS) data base. Moreover, a detailed structural analysis of the synthesized materials was performed by XRD. Crystalline structures were refined with the Rietveld method by using the BGMN program [32] and the graphical interface Profex [33]. Peak profiles were modeled with a Lorentzian function to determine the crystal size anisotropy using the Debye-Scherrer formula [34] and spherical harmonics as base functions to model the reflection width parameters, as a function of the reflection Miller indices.

The powder average particle size and morphology were analyzed using scanning and transmission electron microscopies. SEM analysis was performed on a JEOL JMS-7600F and the TEM images were obtained on a JEOL JEM 1200EX. Electron diffraction analysis was obtained, and the interplanar distances (*d*) were obtained using $dR = \lambda L$ equation; where, *R* is the radius of the rings of the diffraction pattern, *L* the constant of the camera (100 cm) and λ is the wavelength (0.0034 Å-120 V).

Moreover, textural features of the samples, including specific surface area, were estimated by nitrogen adsorption-desorption measurements. The nitrogen adsorption-desorption isotherms of the LiAlO₂ powders heat-treated at different temperatures were obtained on a Bel-Japan Minisorp II instrument at 77 K using a multipoint technique (N₂ from Praxair, grade 4.8). Prior to this analysis, each sample was degassed at room temperature for 24 h in vacuum. The surface area was determined using the Brunauer-Emmett-Teller (BET) model.

Results and discussion

Chemistry of the gel precursor

As mentioned in the introduction section, the goal of the EDTA-citrate complexing method is to control the oxide phase formation starting from a homogeneous aqueous phase, wherein the chelating agents modify the aqueous hydrolysis chemistry of the involved metal ions (Li⁺ and Al³⁺) to form stable metal complexes and subsequently give place to a stable gel precursor. Then, as the first stage of the synthesis is related to the

precursor chemistry (from the point of view of the involved metal cations) as well as the complexes formation reactions in terms of pH and chelating agents' concentration among other variables; the construction and analysis of the chemical equilibrium diagrams is an important source of information. Therefore, the equilibrium diagrams were constructed by using the Hydra-Medusa software [35]. Fig. 1 shows the chemical species in the studied system, considering pH range values from 2 to 14. The concentrations of the Li^+ , Al^{3+} , citrate (cit^{3-}) and EDTA^{4-} are 100, 100, 200 and 300 mM respectively, where the latest agrees with the correspondent molar ratio of 1:1:1.5 for metal cations: citric acid: EDTA experimentally studied. Fig. 1(A) shows the distribution of ionic lithium containing species. Briefly, at pH values at around 9, the concentration of the different species is as follows: $[\text{Li}(\text{Cit})^{2-}] > [\text{Li}(\text{EDTA})^{3-}] > [\text{Li}^+]$. On the other hand, Fig. 1(B) shows the distribution of aluminum containing ionic species. In this case, complexes are mainly formed with the EDTA, and the concentration of the different species is as follows: $[\text{Al}(\text{EDTA})\text{OH}^{2-}] > [\text{Al}(\text{EDTA})(\text{OH})_2^{3-}] > [\text{Al}(\text{EDTA})^-]$. In this case; at the pH of 9, aluminum cations are hydroxylated as $\text{Al}(\text{OH})_3$, where it is less prone to form complexes with the citric acid.

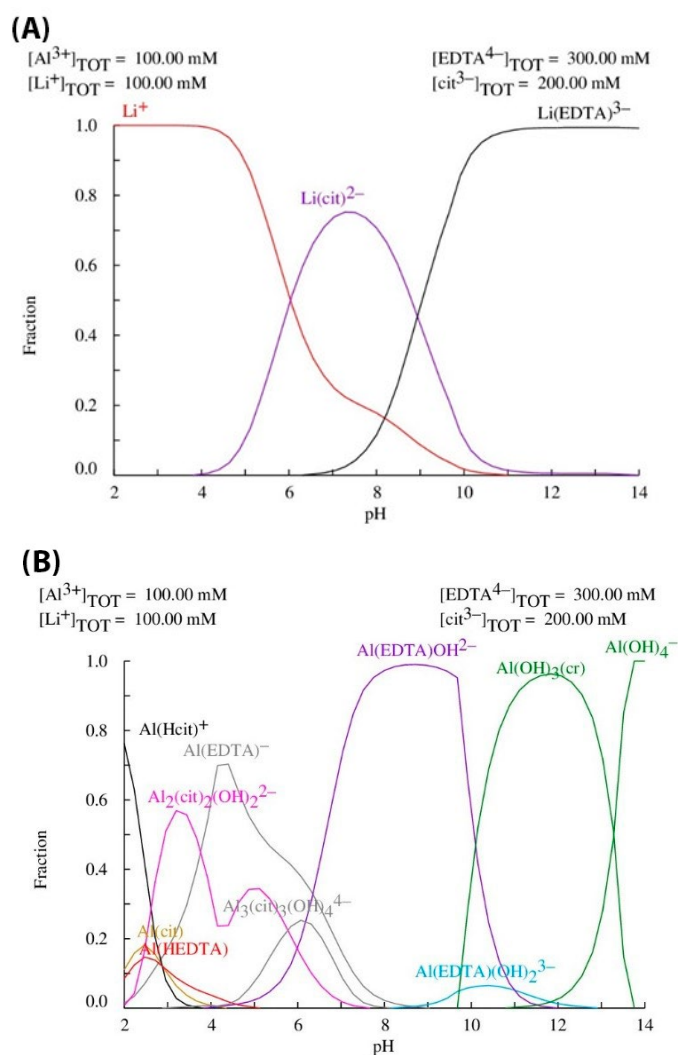
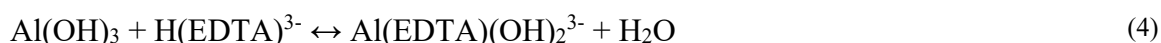
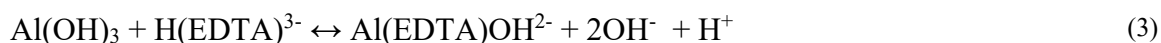


Fig. 1. Distribution diagrams of metal ions containing species among EDTA and citrate complexes as a function of pH: (A) lithium cations and (B) aluminum cations.

Based on the gel precursor chemical composition and considering the basic complexation theory of EDTA and citrate [36,37], the possible formation of different species could be taking place as follows (reactions 1-5).



It should be noticed that equilibrium diagrams show that when the pH decreases below 9 the formation of complexes involving lithium is less effective, giving place to the presence of free metal ions (Li^+) in the resulting co-ordination solution. On the contrary, if the pH increases beyond ~ 9.6 , aluminum tends to form $\text{Al}(\text{OH})_3$ precipitates. Therefore, equilibrium diagrams point out that pH about 9 promotes the formation of a stable and compositional homogeneous gel precursor.

Formation of complexing precursor

The presence of the different species in the gel precursor was characterized by FT-IR spectroscopy. Fig. 2 shows the spectrum of the obtained fresh gel (before self-combustion). As expected, the FT-IR spectrum indicates the presence of hydroxyl groups with vibration bands at 3423 and 3181 cm^{-1} , which can be assigned to the stemming from carboxyl species and water [38-40]. Moreover, the vibration band at 1616 cm^{-1} and the small vibration band around 1385 cm^{-1} are due to bending vibrations of the molecular water and the nitrates in the precursor, respectively.

Different to the vibration bands of the carboxyl groups for both the free citric acid (CA) and the free EDTA, which have been reported to occur in the range from 1650 and 1800 cm^{-1} [41]; this spectrum shows those carboxyl vibration bands situated at 1409 and 1579 cm^{-1} assigned to the vibration of the coordinated carboxyl groups from the complexing agents (CA and EDTA), but after chelating with the metal ions. This behavior has been reported for the case of complexes formed between CA and EDTA with Y^{3+} and Li^+ [38, 41]. Actually, according to the reported data different to the free carboxylic group; the metal ions complexing formation results in a difference between the asymmetric $\nu_a \text{ COO}^-$ and symmetric $\nu_s \text{ COO}^-$ stretching vibrations of about 178 cm^{-1} . Here, $\Delta\nu$ is 170 cm^{-1} in agreement with the Kakihana's criteria [42, 38]. Moreover, the small shoulder observed at 1712 and the vibration band centered at 1264 cm^{-1} have been reported due to the Li/CA complex formations [42]. Specifically, the latter appears when CA-carboxyl acts as a monodentate ligand with lithium and it is assigned to the ν_s of the COO^- group. Moreover, the vibration bands at 1409 and 1099 cm^{-1} are due to ν_s (C-O) and ν_a (C-N) bonds after Al/EDTA complexing [40].

Considering the stability constants for the complex formation the distinctly higher value for $\text{Al}^{3+}/\text{EDTA}$ constant ($\log K = 16.1$) in comparison with the Al^{3+}/AC system ($\log K = 11.7$), make a complexation of this cation with EDTA most likely [36]. In the Li^+ cation case; the complex formation has a value of $\log K = 2.79$ enabling the complex formation. However, there were not found, in literature, additional information regarding the Li^+/AC system. All these results not only support the information displayed in the constructed equilibrium diagrams, wherein it is suggested the initial formation of Li/CA and Li/EDTA species and the preferential formation of Al/EDTA complexes, proving that chelation takes place successfully by the combined EDTA-citrate complexing method. This is particularly important from the point of view that the conversion of the gel precursor to the oxide phase still involves a calcining stage, and therefore the obtaining of an organic matrix wherein the metal complexes are distributed ensuring the chemical homogeneity of the system at atomic scale for obtaining of the pure oxide phase and fine particles [31]. Further, FT-IR analysis reveals several

vibration bands in the range from 400-900 cm^{-1} , which may be identified to the Al-O and Li-O vibrations in the structural groups AlO_6 , LiO_6 , AlO_4 and LiO_4 of different lithium aluminate species [43-46]. Specifically, vibration bands at 556, 660 and 808 cm^{-1} indicate the presence of $\gamma\text{-LiAlO}_2$ [43-45], while vibration bands at 438, 496, 629 and 696 cm^{-1} can be assigned to LiAl_3O_8 . Therefore, FT-IR analysis reveals the presence of M-O binding in the precursor. Finally, the vibration band at 745 cm^{-1} can be attributed to the presence of aluminum hydroxide.

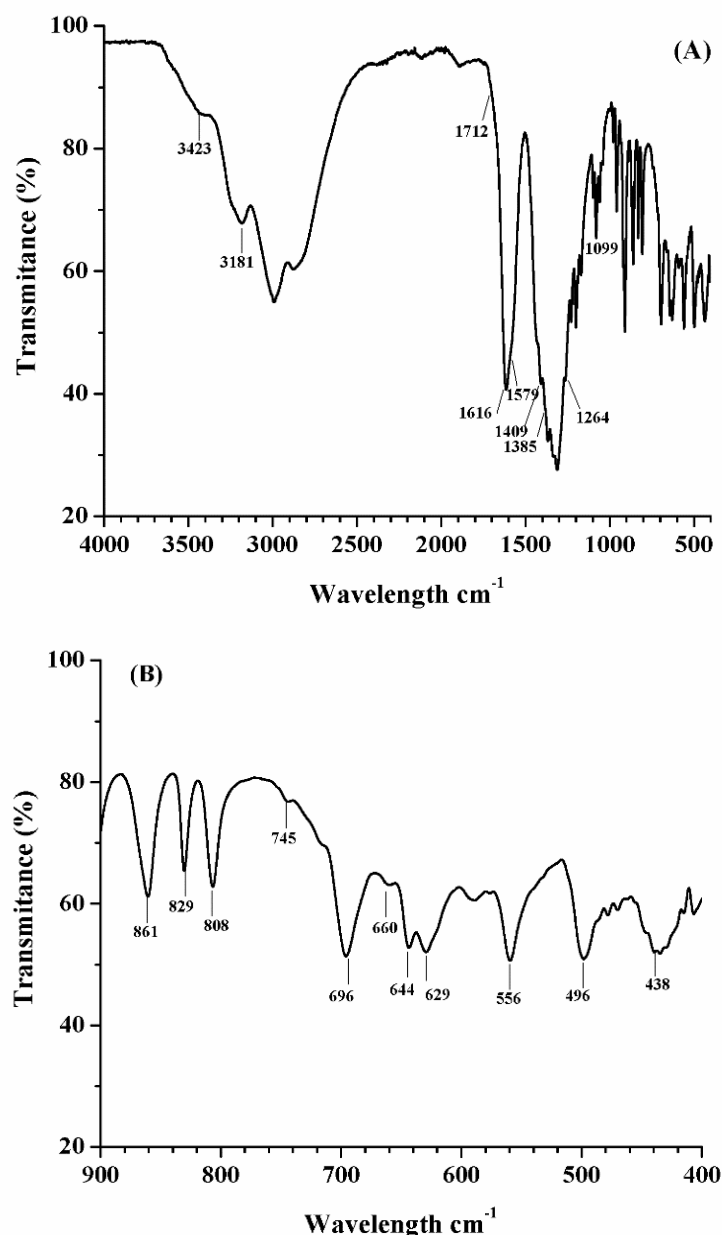


Fig. 2. FT-IR spectrum for the fresh gel precursor (before self-combustion stage): (A) whole spectrum range from 400-4000 cm^{-1} and (B) spectrum range from 400-900 cm^{-1} .

Thermal behavior of complexing precursor

The evolution of the gel sample towards the formation of γ -LiAlO₂ was analyzed by TG-DTA. Fig. 3 shows the obtained thermograms, exhibiting a thermal multi-stage decomposition (TG) behavior of the incipient dried gel with the corresponding endo and exothermic (DT) processes. Thermogravimetric results reveal a small mass loss of about 3.5 wt% between 40 and 140 °C. Due to the temperature range, this fact was attributed to loss of moisture in the sample. Then, a second mass loss of about 34 wt% occurs between 140 and 305 °C. This weight loss is accompanied by an endothermic peak at 192 °C (DTA curve) caused by the removal of the compositional water and other solvents (such as NH₄OH) trapped in the gel. Subsequently, a third mass loss of 8.5 wt% takes place from 305 to 412 °C suggesting the beginning of the organic precursor decomposition; as well as remained nitrates; this third mass loss correspond to a small exothermic peak at 360 °C (DTA curve). The thermogram profile is certainly complex and shows that stable intermediates are not formed. Finally, there is also another abrupt weight loss of about 23 wt% in the temperature range of 412-560 °C; simultaneously, an exothermic peak (DTA curve) appears at 503 °C, which must correspond to the decomposition of the residual organic compounds by combustion. There are no additional weight changes nor heat flow events beyond 560 °C. Therefore, at this temperature, the residual sample is the oxide material.

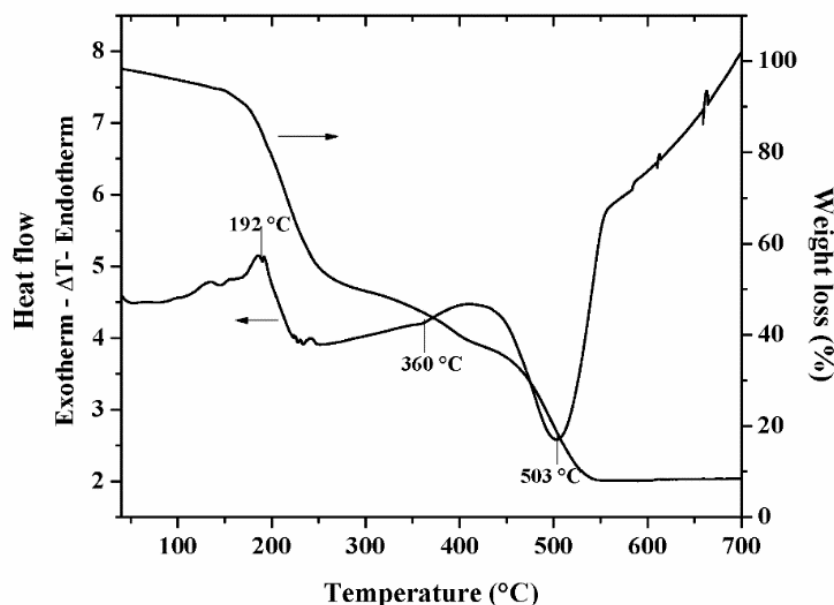


Fig. 3. Thermogravimetric and differential thermal analysis (TG-DTA), simultaneously performed on fresh gel precursor sample.

Formation and characterization of lithium aluminate powders

After the thermal analysis, XRD was conducted to elucidate the effect of calcination temperature during LiAlO₂ formation. Actually, lithium monoaluminate has different polymorphic phases and the pathway of crystallization may show differences regarding the synthesis route and precursors [47,48]. Fig. 4 shows the XRD patterns of all the heat-treated samples from 600 to 900 °C, where the initial temperature was based on the thermal analysis. The XRD pattern of the as-burnt sample was included for comparison purposes.

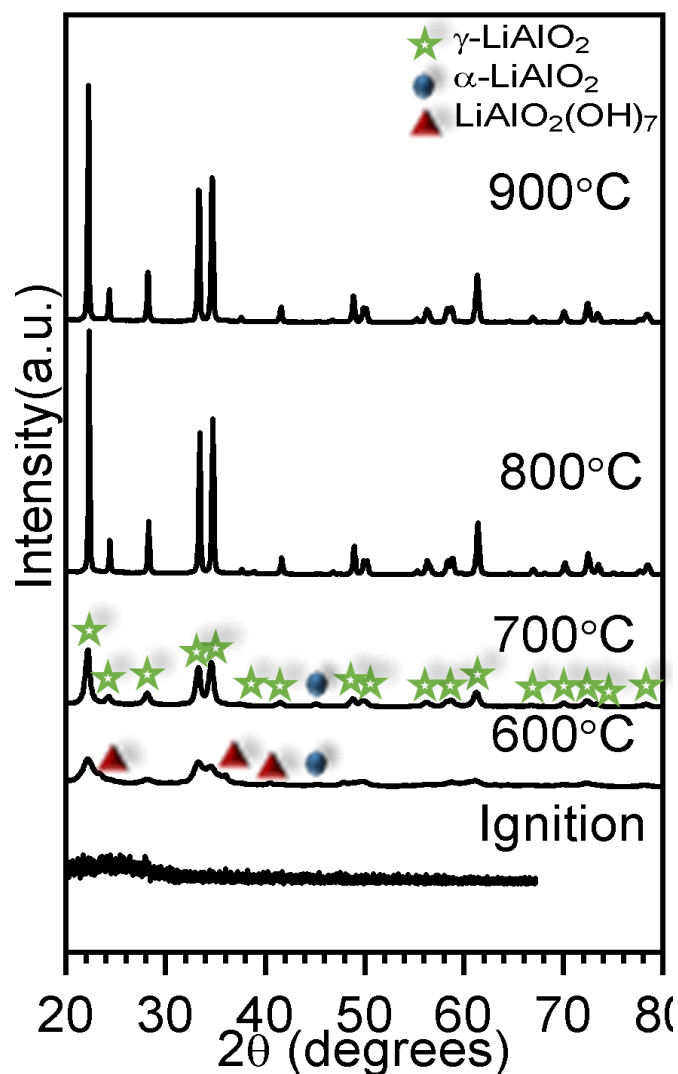


Fig. 4. XRD patterns of calcined materials between 600 and 900 °C. The as-burnt sample was included for comparison purposes (ignition).

In Fig. 4, XRD analysis of the as-burnt sample shows an amorphous phase; and according with TG-DTA results, the presence of the well crystallized oxide phases free of organics was evidenced only in the samples heat treated at high temperatures. However, it is important to have in mind that FT-IR analyses evidenced the obtaining of species containing M-O binding, even before calcining. Moreover, at 600 and 700 °C the XRD patterns evidenced the formation of γ -LiAlO₂ (JCPDS # 38-1464) with lithium aluminum hydroxide hydrated (LiAl₂(OH)₇·H₂O) and α -LiAlO₂, as minority secondary phases. These observed secondary phases were identified with the JCPDS 40-0710 and 74-2232 files respectively. Of course, the presence of LiAl₂(OH)₇·H₂O must have been produced by a hydroxylation process produced during the environmental sample exposition. The pure γ -LiAlO₂ phase is obtained at temperatures above 700 °C. Hence, it is clear that there is change on the XRD patterns profile as a function of temperature (peak broadening decreased as temperature increased), where the γ -LiAlO₂ crystal size increases. Therefore, to further analyze these samples by XRD, heat-treated samples were refined by the Rietveld method. Fig. 5 shows the Rietveld refinement results

obtained for the four heat-treated samples, where γ -LiAlO₂ or mixtures of α -LiAlO₂, γ -LiAlO₂ and LiAl₂(OH)₇H₂O were modeled. All the initial crystallographic data was available in previous reports [49-51]. In all cases, Rietveld analyses fitted very well with the corresponding sample.

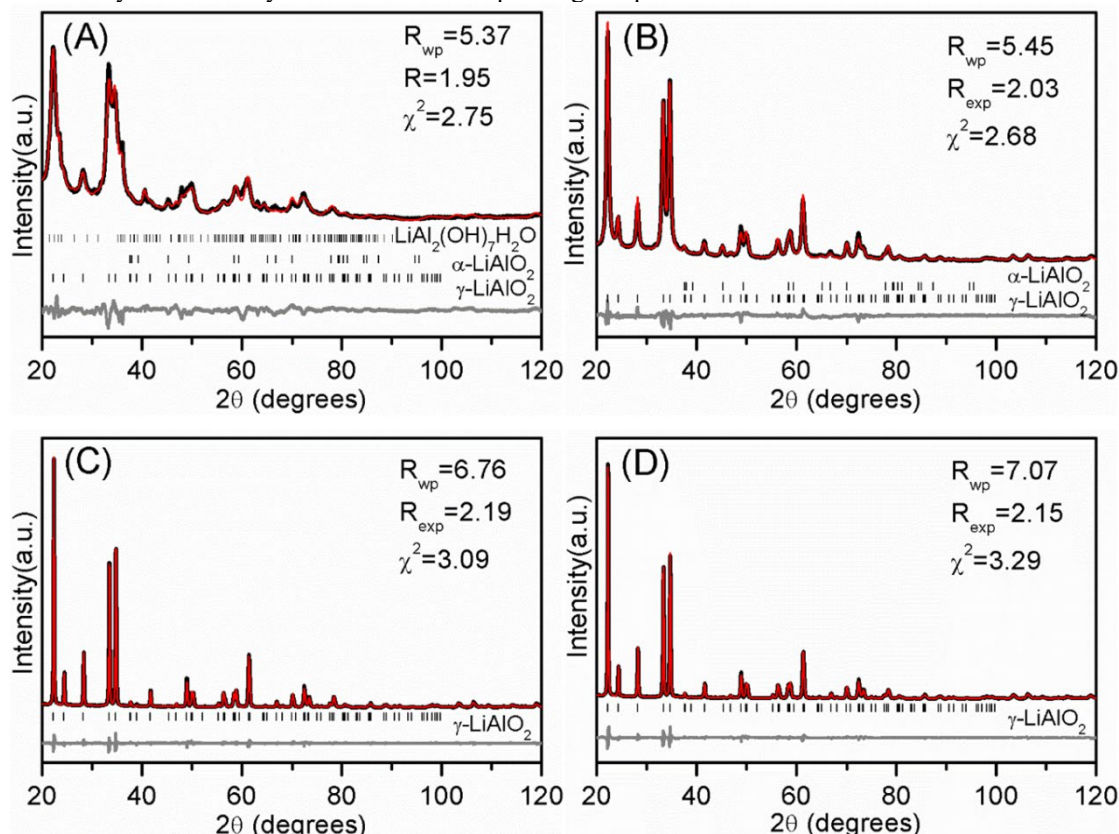


Fig. 5. XRD Rietveld analysis of samples calcined at different temperatures (A)600, (B) 700, (C) 800 and (D) 900 °C. The continuous black lines are experimental data and red superposed lines are calculated patterns. At the bottom of each diagram, the difference between experimental and calculated points is shown (gray). Vertical marks are the Bragg positions for different crystalline phases.

Table 1 shows the final γ -LiAlO₂ lattice parameters obtained as a function of temperature, where Li and Al positions were refined on x, due to their crystallographic symmetry. As it can be seen, at 700 °C and higher temperatures, none of the lattice parameters presented significant variations, demonstrating the high γ -LiAlO₂ structural stability as a function of temperature, which is an important feature on the nanoparticles synthesis.

Table 1. γ -LiAlO₂ lattice parameters and atom coordinates Al_x, Li_x, O_{x,y,z} as a function of sample annealing temperature.

T(°C)	a (nm)	c (nm)	Al _x (fracc.)	Li _x (fracc.)	O _x (fracc.)	O _y (fracc.)	O _z (fracc.)
600	0.5177(3)	0.6273(4)	0.1677(7)	-0.227(3)	0.206(1)	-0.179(1)	0.0316(7)
700	0.5190(2)	0.6301(2)	0.1726(2)	-0.173(1)	0.2122(4)	-0.1694(4)	0.0201(3)
800	0.51790(6)	0.62910(7)	0.1755(1)	-0.1843(7)	0.2108(2)	-0.1639(3)	0.0224(2)
900	0.51810(6)	0.62997(8)	0.1756(2)	-0.1861(8)	0.2102(2)	-0.1635(6)	0.0223(2)

As a part of the Rietveld analysis, phase concentration percentages and crystal sizes were determined as a function of the annealing temperature. In the first case, the phase concentration analysis confirmed that γ -LiAlO₂ was obtained pure at temperatures equal or higher than 700 °C, and at lower temperatures α -LiAlO₂ and lithium aluminum hydroxide were presented as secondary phases (Table 2). In the other case, γ -LiAlO₂ crystal size was determined using different crystallographic planes, where all of them showed homogeneous crystal growths, in other words, it was obtained equiaxial crystals (Table 3). While γ -LiAlO₂ obtained at 600 and 700 °C presented crystal sizes between 6.6 and 16.6 nm, the pure γ -LiAlO₂, obtained at 800 and 900 °C, presented crystal sizes of around 110 nm. Moreover, the crystal size did not really evidence an important growth when γ -LiAlO₂ was calcined at 800 or 900 °C.

Table 2. Phase concentration (wt%) as a function of sample annealing temperature.

T (°C)	γ -LiAlO ₂	α -LiAlO ₂	LiAl ₂ (OH) ₇ •H ₂ O
600	78.8(5)	5.4(2)	15.8(5)
700	96.62(9)	3.38(9)	0
800	100	0	0
900	100	0	0

Table 3. γ -LiAlO₂ average crystal size in different crystallographic directions, as a function of sample annealing temperature.

T(°C)	Crystal size (nm)		
	(200)	(012)	(111)
600	6.6(2)	8.1(2)	7.0(1)
700	16.6(1)	16.6(1)	16.61(8)
800	110(3)	115(4)	111(7)
900	107(3)	113(5)	110(2)

In addition to the structural characterization, the four samples were microstructurally analyzed by N₂ adsorption-desorption and SEM techniques. The N₂ adsorption-desorption isotherms of all γ -LiAlO₂ samples presented isotherms type II, corresponding to non-porous materials [52], where the whole N₂ volume adsorptions decreased as a function of temperature (Fig. 6). Moreover, isotherms obtained from samples treated at 600 and 700 °C presented a very narrow H3 hysteresis loops. In these cases, hysteresis must be associated to particle agglomeration, instead of porous formation. Based on previous results, specific surface area was determined by the BET model, obtaining values of 72.5, 38.7, 5.4 and 3.1 m² g⁻¹ for the samples heat treated at 600, 700, 800 and 900 °C, respectively.

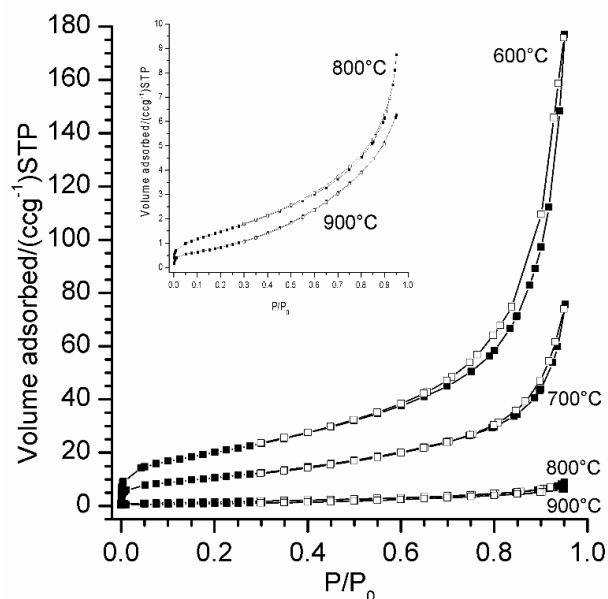


Fig. 6. N_2 adsorption-desorption isotherms of γ -LiAlO₂ powders calcined at different temperatures. All N_2 adsorption-desorption curves presented isotherms type II, corresponding to non-porous materials. The square inset shows an amplification of the N_2 adsorption-desorption isotherms obtained for the samples calcined at 800 and 900 °C.

Fig. 7 shows the secondary electron images of γ -LiAlO₂ samples thermally treated at different temperatures, where it can be seen an important morphological evolution. In the γ -LiAlO₂ samples treated at 600 and 700 °C (Figures 7(A) and (B), respectively) it can be observed the presence of large agglomerates formed by nanometric particles, where their ultimate particle sizes cannot be resolute. In these cases, only non-homogeneous surfaces can be described; although γ -LiAlO₂ sample treated at 700 °C (Fig. 7(B)) seemed to present a denser particle arrangement. On the contrary, secondary electron images of γ -LiAlO₂ samples treated at 800 and 900 °C (Figures 7(C) and (D)) clearly defined their morphological characteristics. γ -LiAlO₂ sample treated at 800 °C (Fig. 7(C)) presented polygonal particles of 160 nm in average, while sample treated at 900 °C (Fig. 7(D)) presented larger particles (250 nm). From these images, it is evident that γ -LiAlO₂ sample morphology remarkably changed as a function of temperature, as the particle sizes growth from a few nanometers at 600 °C to 250 nm at 900 °C. Hence, microstructural analyses (specific surface area and particle size) varied as a function of temperature, as it could be expected. All these results are in good agreement, indirectly, to crystal size growth determined by Rietveld.

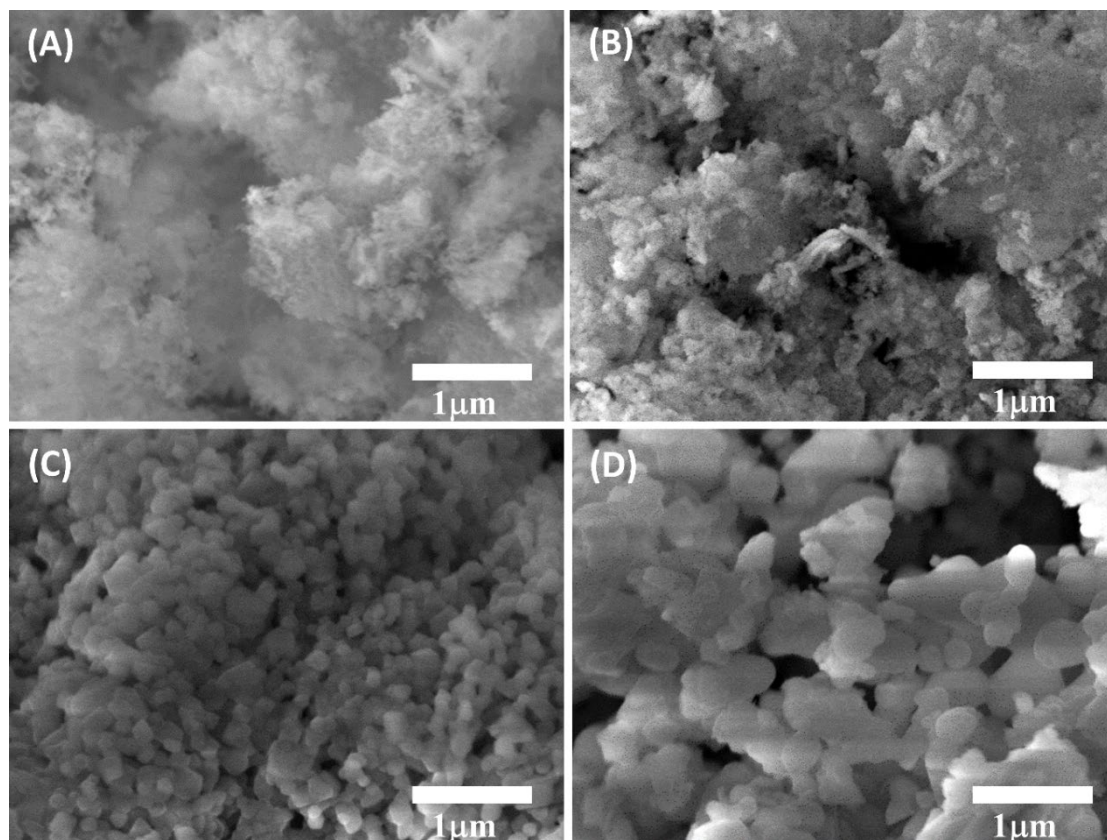


Fig. 7. SEM images of γ -LiAlO₂ powders calcined at 600, 700, 800 and 900°C.

In order to deeply analyze the γ -LiAlO₂ characterization, a transmission electron microscopy analysis was performed on all of these samples. Fig. 8 shows bright-field images of γ -LiAlO₂ samples, where samples presented an important evolution as a function of temperature, as in the scanning electron microscopy analysis. γ -LiAlO₂ sample treated at 600 °C (Fig. 8(A)) shows very tiny particles of around 5 nm. In fact, particle size growth as a function of the γ -LiAlO₂ annealing process, from around 25 nm to 120-150 nm at 700 and 900 °C, respectively. This systematic growth is in very good agreement with crystal size evolution determined by Rietveld analysis (see Table 3). Moreover, this result suggests that the observed ultimate nanoparticles are single crystals.

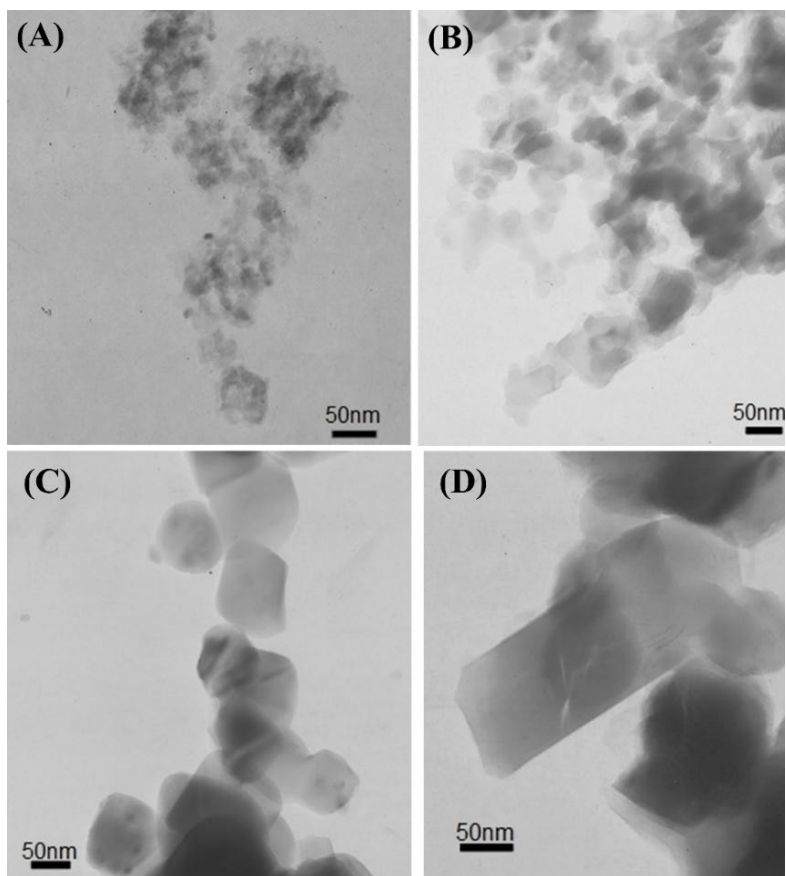


Fig. 8. TEM images of γ -LiAlO₂ powders calcined at 600 (A), 700 (B), 800 (C) and 900 °C (D).

Finally, TEM and XRD results were correlated by the electron diffraction pattern of γ -LiAlO₂ sample heat-treated at 900 °C. Fig. 9 and Table 4 show the interplanar distances measured from the electron diffraction ($[\bar{1}11]$ zone of γ -LiAlO₂) and XRD Rietveld analysis, where both analyses show an excellent agreement. All these results demonstrate that γ -LiAlO₂ synthesis by the EDTA-citrate complexing method can produce pure and crystalline nanoparticles, which would be of interest in different applications that demand phase purity and particle size control.

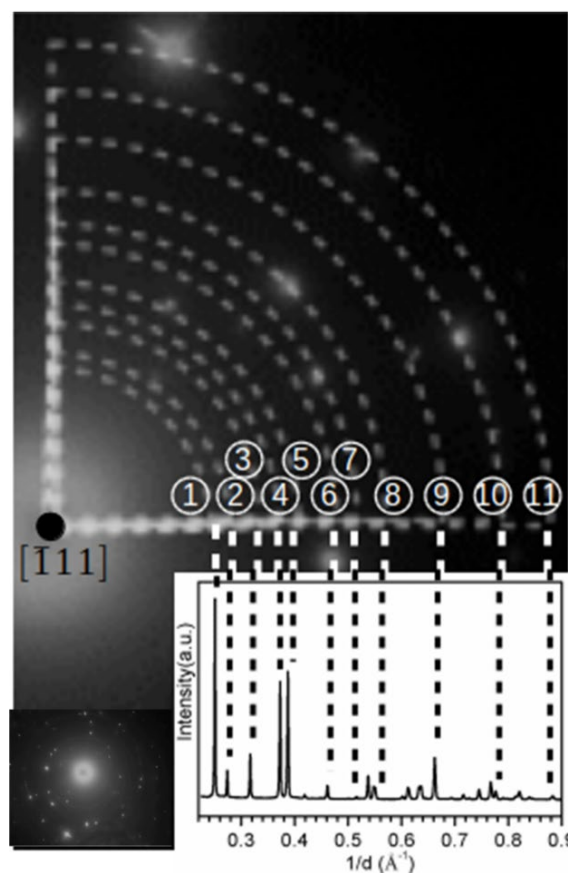


Fig. 9. Correlation between electron diffraction pattern, obtained by TEM, and XRD pattern of the pure γ -LiAlO₂ sample heat-treated at 900 °C.

Table 4. Interplanar distances obtained from XRD-Rietveld and TEM analyses for γ -LiAlO₂ heat-treated at 900 °C.

Peak labeled at Fig. 9	d obtained by XRD-Rietveld, (Å)	d obtained by TEM, (Å)	(hkl)
1	4.002	4.002	101
2	3.663	3.602	110
3	3.167	3.005	111
4	2.691	2.701	012
5	2.590	2.513	200
6	2.175	2.161	211
7	1.946	1.965	103
8	1.759	1.757	221
9	1.507	1.501	104
10	1.292	1.294	313
11	1.139	1.137	332

Conclusion

Gamma lithium aluminate (γ -LiAlO₂) nanoparticles was successfully synthesized at low temperature by the combined EDTA-citrate complexing method. Using a gel precursor analysis performed by chemical speciation, the synthesis conditions were established. The purity of the γ -LiAlO₂ phase was determined as 97 % at 700 °C and 100 % over this temperature. By calcination at 700 °C, pure lithium aluminate powders exhibit small crystal size of about 16.6 nm, as well as high specific surface area (38.7 m²g⁻¹). Then, at 800 and 900 °C the average crystal size was around 100 nm. Moreover, analyzing by Rietveld method the XRD patterns of samples heat treated at different temperatures, it was observed that none of the γ -LiAlO₂ lattice parameters presented important variations, or new phase formation, demonstrating a high γ -LiAlO₂ structural stability as a function of temperature, which is an important feature on the nanoparticles synthesis. Additionally, γ -LiAlO₂ can present certain microstructural changes as a function of calcination temperature. SEM analysis showed an increase of particle size in agreement, directly to the crystal size growth determined by Rietveld and TEM. Also, electron diffraction patterns showed an excellent agreement between the XRD and Rietveld results.

Generally speaking, results showed that γ -LiAlO₂ synthesis by the EDTA-citrate complexing method can produce pure and crystalline nanoparticles of the oxide, wherein the combination of the chelating agents EDTA-citrate helps to the formation of an initial complexing precursor that promotes the further formation of the pure γ -LiAlO₂ phase without impurities at 700 °C or higher temperatures.

Acknowledgment

This work was supported by Proyectos de Investigación Científica y Desarrollo Tecnológico SIP-IPN No. 20190014. J.A. Fabián thanks to Proyectos de Desarrollo Tecnológico o Innovación para Alumnos 2019, SIP-IPN. Finally, Ortiz-Landeros J. and Ovalle-Encinia O. wish to express their appreciation for the SIBE-IPN and EDI-IPN, and PNPC-CONACYT programs, respectively. We thank Flores-Morales C., for technical help in TEM analyses.

References

1. Wen, Z.; Wu, X.; Xu, X.; Lin, J.; Gu, Z. *Fusion Eng. Des.* **2010**, 85, 551-555.
2. Van der Laan, J.G.; Fedorov, A.V.; Van Til, S.; Reimann, J. *Comprehensive Nucl. Mater.* **2012**, 4, 463-510.
3. Leys, O.; Bergfeldt, T.; Kolb, M.H.H.; Knitter, R.; Goraieb, A. A. *Fusion Eng. Des.* **2016**, 107, 70-74.
4. Peng, Z.D.; Cao, Y.B.; Hu, G.R.; Du, K.; Gao, X.G.; Xiao, Z.W. *Chinese Chem. Lett.* **2009**, 20, 1000-1004.
5. Inaguma, Y.; Nakashima, M. *J. Power Sour.* **2013**, 228, 250-255.
6. Tatsumisago, M.; Takano, R.; Tadanaga, K.; Hayashi, A. *J. Power Sour.* **2014**, 270, 603-607.
7. Alcántara, R.; Ortiz, G.; Tirado, J.L.; Stoyanova, R.; Zhecheva, E.; Ivanova, S. *J. Power Sour.* **2009**, 194, 494-501.
8. Sabikoglu, I.; Ayvacikli, M.; Bergeron, A.; Can, N. *J. Lumin.* **2012**, 132, 1597-1602.
9. Kim, J.S.; Song, H.J.; Roh, H.S.; Yim, D.K.; Noh, J.H.; Hong, K.S. *Mater. Lett.* **2012**, 79, 112-115.
10. Wang, J.X.; Chen, K.T.; Wu, J.S.; Wang, P.H.; Huang, S.T.; Chen, C.C. *Fuel Process Technol.* **2012**, 104, 167-173.
11. Puna, J.F.; Gomes, J.F.; Bordado, J.C.; Correia, M.J.N.; Dias, A.P.S. *Appl. Catal. A.* **2014**, 470, 451-457.
12. Briz-López, E.M.; Ramírez-Moreno, M.J.; Romero-Ibarra, I.C.; Gómez-Yáñez, C.; Pfeiffer, H.; Ortiz-Landeros, J. *J. Ener. Chem.* **2016**, 25, 754-760.

13. Lara-García, H.A.; Ramírez-Moreno, M.J.; Ortiz-Landeros, J.; Pfeiffer, H. *RSC Adv.* **2016**, 6, 57880-57888.
14. Pejchal, J.; Babin, V.; Kucerkova, R.; Mihokova, E.; Beitlerova, A.; Kurosawa, S.; Nikl, M.; Yoshikawa, A. *J. Lumin.* **2018**, 201, 231-244.
15. Pejchal, J.; Fujimoto, Y.; Chani, V.; Yanagida, T.; Yokota, Y.; Yoshikawa, A.; Nikl, M.; Beitlerova, A. *J. Cryst. Growth.* **2012**, 360, 127-130.
16. Antolini, E. *Ceram. Inter.* **2013**, 39, 3463-3478.
17. Rajaa, M.; Sanjeev, G.; Kumar, T.P.; Stephan, A.M. *Ceram. Inter.* **2015**, 41, 3045-3050.
18. Heo, S.J.; Hu, B.; Manthina, V.; Hilmi, A.; Yuh, C.Y.; Surendranath, A.; Singh, P. *Inter. J. Hydrogen Ener.* **2016**, 41, 18884-18892.
19. Gao, J.; Shi, S.; Xiao, R.; Li, H.; *Solid State Ion.* **2016**, 286, 122-134.
20. Yang, X.; Ning, G.; Li, X.; Lin, Y. *Mater. Lett.* **2007**, 61, 4694-4696.
21. Pejchal, J.; Fujimoto, Y.; Chani, V.; Moretti, F.; Yanagida, T.; Nikl, M.; Yokota, Y.; Beitlerova, A.; Vedda, A.; Yoshikawa, A. *J. Crystal Growth.* **2011**, 318, 828-832.
22. Masoud, E.M.; El-Bellihi, A.A.; Bayoumy, W.A.; Mousa, M.A. *Mater. Res. Bull.* **2013**, 48, 1148-1154.
23. Joshi, U.A.; Chung, S.H.; Lee, J.S. *Chem. Commun.* **2005**, 35, 4471-4473.
24. Li, L.; Chen, Z.; Zhang, Q.; Xu, M.; Zhou, X.; Zhu, H.; Zhang, K. *J. Mater. Chem. A.* **2015**, 3, 894-904.
25. Dai, Y.M.; Wu, J.S.; Chen, C.C.; Chen, K.T. *Chem. Eng. J.* **2015**, 280, 370-376.
26. Lin, J.; Wen, Z.; Xu, X.; Gu, Z. *Ceram. Inter.* **2010**, 36, 2221-2225.
27. Jian, C.; Liejin, G.; Shisen, X.; Ruiyun, Z.; Chen, L. *Chinese J. Chem. Eng.* **2012**, 20, 776-783.
28. Li, F.; Hu, K.; Li, J.; Zhang, D.; Chen, G. *J. Nucl. Mater.* **2002**, 300, 82-88.
29. Cushing, B.L.; Kolesnichenko, V.L.; O'Connor, C. *J. Chem. Rev.* **2004**, 104, 3893-3946.
30. Pathak, A.; Pramanik, P. *Proc. Indian NaSci. Acad. A.* **2001**, 67, 47-70.
31. Danks, A.E.; Hall, S.R.; Schnepp, Z. *Mater. Horiz.* **2016**, 3, 91-112.
32. Bergmann, J.; Friedel, P.; Kleeberg, R.; *IUCr commission on powder diffraction newsletter*, **1998**, 20, 5-8.
33. Döbelin, N.; Kleeberg, R. *J. Appl. Crystall.* **2015**, 48, 1573-1580.
34. Klug, M.P.; Alexander, L.E.; *X-ray diffraction procedure for polycrystalline and amorphous materials*, New York, USA: Wiley, 1974.
35. Puigdomenech, I. *Hydra/medusa chemical equilibrium database and plotting software*. KTH Royal Institute of Technology, 2004.
36. Philip, C. H. M. *J. Chem. Edu.* **1997**, 74, 1235-1237.
37. Feldhoff, A.; Arnold, M.; Martynczuk, J.; Gesing, Th. M.; Wang, H. *Solid State Sci.* **2008**, 10, 689-701.
38. Predoana, L.; Jitianu, A.; Preda, S.; Malic, B.; Zaharescu, M. *J. Therm. Anal. Calorim.* **2015**, 119, 145-153.
39. Yu, Hsuan-Fu.; Wang, J.; Wang, Shuen-Shian.; Kuo, Yu-Man. *J. Phys. Chem. Solids.* **2009**, 70, 218-223.
40. Wang, C.; Bai, X.; Liu, S.; Liu, L. *J. Mater. Sci.* **2004**, 39, 6191-6201.
41. Wang, Y. H.; Wang, Z. S.; Jiang, Y.; Wang, X.; Cheng, J.G. *Inter. J. Appl. Ceram. Technol.* **2016**, 13, 736-742.
42. Marques-Ferreira, F.; Motta, M.; Batagin-Neto, A.; De Oliveira- Graeff, C. F.; Lisboa-Filho, P.N.; Lavarda, F.C. *Mater. Res.* **2014**, 17, 550-556.
43. Oksuzomer, F.; Naci-Koc, S.; Boz, I.; Ali-Gurkaynak, M. *Mater. Res. Bull.* **2004**, 39, 715-724.
44. Kutty, T.R.N.; Nayak, M. *Mater. Res. Bull.* **1999**, 34, 249-262.
45. Ananias-Ribeiro, R.; Santana-Mohallen, N.D. *Quim Nova*, **2001**, 24, 773-777.
46. Chatterjee, M.; Naskar, M.K. *J. Mater. Sci. Lett.* **2003**, 22, 1747-1749.
47. Kutty, T.R.N.; Nayak, M.; *Mater. Res. Bull.* **1999**, 34: 249-262.
48. Kharlamova, O.A.; Mitrofanova, R.P.; Tarasov, K.A.; Chupakina, L.P.; Isupov, V.P.; Zyryanov, A.S.; Aleksandrv, K.A.; Batalov, N.N.; Kozlova, Z.R. *Chem. Sustain. Develop.* **2004**, 12, 379-383.

49. Bertaut, E.F.; Delapalme, A.; Bassi, G.; Durif-Varambon, A.; Joubert, J.C. *Bull. Soc. Franc. Min. Cristal.* **1965**, 88, 103-108.
50. Marezio, M.; Remeika, J.P. *J. Chem. Phys.* **1996**, 44, 3143-3144.
51. Thiel, J.P.; Chiang, C.K.; Poeppelmeier, K.R.; *Chem. Mater.* **1993**, 5, 297-304.
52. Sing, K.S.W.; Everett, D.H.; Haul, R.A.W.; Moscou, L.; Pierotti, R.A.; Rouquerol, J.; Siemieniowska, T. Reporting physisorption data for gas/solid systems. *Handbook of heterogeneous catalysis*; Weinheim, Germany, Wiley-VCH Verlag GmbH & Co. KGaA, 2008.